Experimental construction of a W superposition state and its equivalence to the Greenberger-Horne-Zeilinger state under local filtration

Debmalya Das,[*] Shruti Dogra,[†] Kavita Dorai,[‡] and Arvind[§]

Department of Physical Sciences, Indian Institute of Science Education & Research Mohali, Sector 81, Mohali, Manauli P.O. 140306, Punjab, India

(Received 22 April 2015; published 5 August 2015)

We experimentally construct a three-qubit entangled W superposition ($W\bar{W}$) state on an NMR quantum information processor. We give a measurement-based filtration protocol for the invertible local operation (ILO) that converts the $W\bar{W}$ state to the Greenberger-Horne-Zeilinger (GHZ) state, using a register of three ancilla qubits. Further we implement an experimental protocol to reconstruct full information about the three-party $W\bar{W}$ state using only two-party reduced density matrices. An intriguing fact unearthed recently is that the $W\bar{W}$ state, which is equivalent to the GHZ state under an ILO, is in fact reconstructible from its two-party reduced density matrices, unlike the GHZ state. We hence demonstrate that, although the $W\bar{W}$ state is interconvertible with the GHZ state, it stores entanglement very differently.

DOI: 10.1103/PhysRevA.92.022307 PACS number(s): 03.67.Bg, 03.67.Lx, 03.67.Mn

I. INTRODUCTION

Explorations of multiqubit entanglement have unearthed several families of states with curious quantum properties and there have been many attempts in recent years to characterize all the denizens of this quantum zoo [1–3]. The situation becomes complicated for systems of more than two qubits and correspondingly the classification of their entanglement turns out to be more involved [4,5].

Pure entangled states of three qubits fall into two categories, namely, the Greenberger-Horne-Zeilinger (GHZ) class or the W class, under stochastic local operations and classical communication (SLOCC) [6,7] with the maximally entangled GHZ and W states being given by

$$\begin{aligned} |\mathrm{GHZ}\rangle &= \tfrac{1}{\sqrt{2}}(|000\rangle + |111\rangle), \\ |\mathrm{W}\rangle &= \tfrac{1}{\sqrt{3}}(|001\rangle + |010\rangle + |100\rangle). \end{aligned} \tag{1}$$

The entanglement of the GHZ state is fragile under qubit loss; i.e., when any one of the qubits is traced out, the other two qubits become completely disentangled [2,8]. Hence if one of the parties decides not to cooperate, the entanglement resources of the GHZ state cannot be used. In contradistinction to the GHZ state, the W-state residual bipartite entanglement is robust against qubit loss [2].

It has been shown by Linden *et al.* that almost every pure state of three qubits can be completely determined by its two-party reduced density matrices [9]. The two inequivalent entangled states, namely, the W and GHZ states, have contrasting irreducibility features: while GHZ states have irreducible correlations and cannot be determined from their two-party marginals [10,11], W states are completely determined by their two-party marginals [12–14]. Tripartite entanglement has been studied extensively in the context of optics [15–20] and NMR [21–27].

Recently, the entanglement properties of a permutation symmetric superposition of the W state and its obverse $\bar{W} = 1/\sqrt{3}(|011\rangle + |101\rangle + |110\rangle)$ have been characterized [28–30]:

$$\begin{aligned} |W\bar{W}\rangle &= \tfrac{1}{\sqrt{2}}(|W\rangle + |\bar{W}\rangle) \\ &= \tfrac{1}{\sqrt{6}}(|001\rangle + |010\rangle + |011\rangle + |100\rangle + |101\rangle + |110\rangle). \end{aligned} \tag{2}$$

While this state (referred to henceforth as the $W\bar{W}$ state) belongs to the GHZ entanglement class, its correlation information (in contrast to the GHZ state) is uniquely contained in its two-party reduced states. The argument for reconstructing the three-qubit $W\bar{W}$ state from its two-party reduced states runs along lines similar to the original argument of Linden *et al.* [9]. If we assume another state to have the same two-party reduced density matrices as the $W\bar{W}$ state, this constraint can be used to prove that the new state is no different from the original $W\bar{W}$ state [29,30].

In this work we focus on the $W\bar{W}$ state. We provide an explicit measurement-based filtration scheme to filter out the $|\mathrm{GHZ}\rangle$ state from the $W\bar{W}$ state. Further, we experimentally construct and tomograph the $W\bar{W}$ state on an NMR quantum information processor of three coupled qubits. We experimentally demonstrate that the information about tripartite correlations present in this state can indeed be completely captured by its two-party reduced density matrices. We reconstruct the experimental density matrices using complete state tomography and compare them with the theoretically expected states and also compute state fidelities. The GHZ class of states are an important computational resource [1] and it has been shown that states that are SLOCC equivalent to these can be used for the same kind of quantum information processing tasks [2]. Therefore, it is expected that the $W\bar{W}$ state will also prove useful for quantum computation. Furthermore, the quantification of the tripartite correlation information present in this state is easier as compared to the GHZ state, as entanglement measurement requires only two-qubit detectors.

The paper is organized as follows. Section II describes how we obtain the GHZ state from the $W\bar{W}$ state by local

[*]debmalya@iisermohali.ac.in
[†]shrutidogra@iisermohali.ac.in
[‡]kavita@iisermohali.ac.in
[§]arvind@iisermohali.ac.in

filtration based on projective measurements using a register of three ancilla qubits. Section III describes the experimental creation of the $W\bar{W}$ superposition state on a three-qubit NMR quantum information processor. Section III A contains the details of the molecule used, the NMR pulse sequence for $W\bar{W}$ state construction and the results of state tomography. The information content of the $W\bar{W}$ state as captured from its two-party marginals is described in Sec. III B. We conclude in Sec. IV with some remarks about GHZ and $W\bar{W}$ types of three-qubit entanglement and the relationship between the entanglement class and how information about entanglement is stored in a quantum state.

II. FILTRATION PROTOCOL TO SHOW THE SLOCC EQUIVALENCE OF $W\bar{W}$ AND GHZ

Measurement-based local filters have been used for entanglement manipulation in the context of violation of Bell inequalities as well as for the detection of bound entangled states [31–33]. No local operations can convert a state from the GHZ class to the W class. However, surprisingly, it has been shown that the $W\bar{W}$ state is in the GHZ class, deriving from the fact that it is related to the GHZ state via the SLOCC class of operations given by [29,30]

$$|\mathrm{GHZ}\rangle \equiv A \otimes A \otimes A |W\bar{W}\rangle, \tag{3}$$

with

$$A = \frac{1}{\sqrt{3}} \begin{pmatrix} 1 & \omega \\ 1 & \omega^2 \end{pmatrix} \tag{4}$$

being an invertible local operation (ILO), where $\omega = e^{\iota \frac{2\pi}{3}}$ denotes the cube root of unity. We have used "$\equiv$" instead of an equality sign in Eq. (3) because A is a nonunitary operator that does not preserve the norm and the two sides in Eq. (3) do not have the same norm.

We now proceed to reinterpret A as an action on an ensemble of identically prepared $W\bar{W}$ states and implement the operation described in Eq. (3). In this process, we will have to discard some copies and the new ensemble that we construct with each member in the filtered GHZ state will have fewer copies as compared to the original ensemble of $W\bar{W}$ states. These aspects will be brought out more clearly when we describe the measurement-based filtration protocol to realize the ILO.

Since A acts on each of the qubits locally, we first want to realize the operation A on a single qubit. The nonunitary operator A has a singular valued decomposition,

$$A = UDV, \tag{5}$$

where the unitary operators U and V are given by

$$U = \frac{e^{\iota\frac{\pi}{2}}}{\sqrt{2}} \begin{pmatrix} e^{-\iota\frac{\pi}{6}} & -e^{\iota\frac{\pi}{3}} \\ e^{\iota\frac{\pi}{6}} & -e^{-\iota\frac{\pi}{3}} \end{pmatrix}, \quad V = \frac{1}{\sqrt{2}} \begin{pmatrix} -\iota & \iota \\ \iota & \iota \end{pmatrix}, \tag{6}$$

and the nonunitary diagonal operator D is given by

$$D = \begin{pmatrix} 1 & 0 \\ 0 & \frac{1}{\sqrt{3}} \end{pmatrix}. \tag{7}$$

The operators U and V are unitary and can be implemented via a local Hamiltonian evolution. Therefore, we now turn to the implementation of D on a one-qubit state.

From the two columns of the operator D we define two vectors:

$$|u_1\rangle = \begin{pmatrix} 1 \\ 0 \end{pmatrix} \quad \text{and} \quad |u_2\rangle = \frac{1}{\sqrt{3}} \begin{pmatrix} 0 \\ 3^{\frac{1}{4}} \end{pmatrix}. \tag{8}$$

These vectors are orthogonal to each other but are not normalized. We now extend the Hilbert space of the system by adding an ancilla qubit. We extend the vectors u_1 and u_2 to the composite Hilbert space formed by the ancilla and the system to obtain two four-dimensional vectors:

$$|\xi_1\rangle = \begin{pmatrix} 1 \\ 0 \\ 0 \\ 0 \end{pmatrix} \quad \text{and} \quad |\xi_2\rangle = \frac{1}{\sqrt{3}} \begin{pmatrix} 0 \\ 3^{\frac{1}{4}} \\ 0 \\ \sqrt{3-\sqrt{3}} \end{pmatrix}. \tag{9}$$

The vectors $|\xi_1\rangle$ and $|\xi_2\rangle$ are not only mutually orthogonal but also normalized.

Using these orthonormal vectors $|\xi_1\rangle$ and $|\xi_2\rangle$, we construct the orthogonal projectors P_1 and P_2:

$$\begin{aligned} P_1 &= |\xi_1\rangle\langle\xi_1| = \begin{pmatrix} 1 & 0 & 0 & 0 \\ 0 & 0 & 0 & 0 \\ 0 & 0 & 0 & 0 \\ 0 & 0 & 0 & 0 \end{pmatrix}, \\ P_2 &= |\xi_2\rangle\langle\xi_2| = \frac{1}{\sqrt{3}} \begin{pmatrix} 0 & 0 & 0 & 0 \\ 0 & 1 & 0 & \sqrt{\sqrt{3}-1} \\ 0 & 0 & 0 & 0 \\ 0 & \sqrt{\sqrt{3}-1} & 0 & \sqrt{3}-1 \end{pmatrix}. \end{aligned} \tag{10}$$

We define the projection operator $P = P_1 + P_2$. The effect of the projector P on the composite system of the single qubit and a one-qubit ancilla turns out to be

$$P = \left(\begin{array}{c|c} D & \Delta \\ \hline \Delta & D' \end{array} \right)_{4\times 4}, \tag{11}$$

where D is the diagonal part of the singular value decomposition of the operator A given in Eq. (7), the complementary matrix $D' = I - D$, and the matrix Δ can be obtained readily from Eq. (10).

If we prepare the ancilla in the state $|0\rangle\langle 0|$ with the system being in an arbitrary state ρ, the action of P on the composite system is given by

$$P(|0\rangle\langle 0| \otimes \rho)P = \left(\begin{array}{c|c} D\rho D & D\rho\Delta \\ \hline \Delta\rho D & \Delta\rho\Delta \end{array} \right). \tag{12}$$

If we measure the projector P on the composite system (system and ancilla), whenever the measurement gives a positive answer, the state after measurement is given by the right-hand side of Eq. (12). We retain only these cases and discard the state whenever the outcome of the measurement is negative. Further, on the final state given in Eq. (12), we measure the projector $|0\rangle\langle 0|$ on the ancilla alone. As before, if the outcome is positive we retain the state, and if the outcome is negative we discard the state. In the case where the outcome is positive, the resultant state is $|0\rangle\langle 0| \otimes D\rho D$ and upon discarding the ancilla we get the state of the system to be $D\rho D$. This completes the application of the nonunitary invertible operator D on ρ. Sandwiching this operation between the

unitary transformations U and V as given in Eq. (5), we achieve the application of the ILO operator A on ρ.

The scheme is easily extendable to $2 \otimes 2 \otimes 2$ systems, where we locally implement A on each of the three qubits. We imagine that the tripartite system is divided between Alice, Bob, and Charlie and each of them can perform local operations at their location. We begin with the state $|W\bar{W}\rangle$ for the three qubits, attach a one-qubit ancilla to each qubit, and measure the local projector P for each qubit. If the outcome of these measurements (which amount to a measurement of $P \otimes P \otimes P$) is positive we retain the state, otherwise we discard the state. Then on each ancilla, we measure the projector $|0\rangle\langle 0|$ and retain the cases in which all the outcomes are positive. Upon discarding the ancillas, the resultant state is the application of D on each qubit. When we sandwich this process between the unitaries U and V on each qubit, we get the final state as $|\mathrm{GHZ}\rangle$. This process of measurement-based filtration is schematically explained in Fig. 1. To decide when to discard and when to retain the outcome, we require classical communication between Alice, Bob, and Charlie. Since we discard the output state in a number of cases, the size of the ensemble obtained in the end is smaller than the size of the original ensemble.

The reason that we have to discard a number of cases is connected with the nonunitary nature of the operation. Since the operation is not unitary, it can be implemented only probabilistically and therefore discarding some of the cases is inevitable. The outcome of the measurement of $P \otimes P \otimes P$ in the affirmative, followed by the affirmative outcome of the measurement of $|0\rangle\langle 0|$ for each of the ancilla qubits, indicates that the operation D has been implemented successfully. For the cases when the answer is not affirmative for any one or more of the measurements, the output state is not the desired state and we discard the same. This is the reason that the process is called a filtering process.

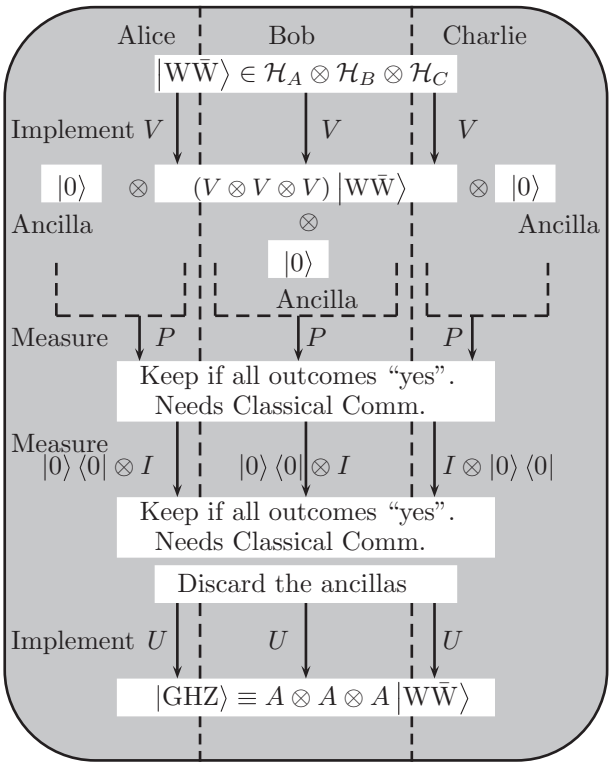

FIG. 1. Schematic diagram of the filtration scheme to implement the nonunitary ILO transformation that converts a $W\bar{W}$ state to a GHZ state.

III. NMR IMPLEMENTATION

To prepare the $W\bar{W}$ state on a three-qubit NMR quantum information processor, we employ the three fluorine (spin-1/2) qubits of trifluoroiodoethylene. The molecular structure and NMR parameters of this three-qubit system are adequate for the kind of manipulations involved in quantum state preparation and are given in Fig. 2(a). Average fluorine longitudinal T_1 relaxation times of 5.0 s and T_2 relaxation times of 1.0 s were experimentally determined. The equilibrium fluorine NMR spectrum obtained after a $\frac{\pi}{2}$ readout pulse is shown in Fig. 2(b).

The system was first initialized into the $|000\rangle$ pseudopure state using the standard spatial averaging technique [34], with the density matrix given by

$$\rho_{000} = (1-\epsilon)\rho_{\mathrm{I}} + \epsilon|000\rangle\langle 000| \tag{13}$$

with a thermal polarization of $\epsilon \approx 10^{-5}$ and $\rho_{\mathrm{I}} = I/8$ being a normalized 8×8 identity operator. NMR is an ensemble technique dealing with zero trace observables and only the deviation density matrix can be experimentally observed. The pure (pseudopure) state in Eq. (13),

$$|000\rangle\langle 000| = \frac{1}{\epsilon}\rho_{\mathrm{dev}} + \rho_{\mathrm{I}}, \tag{14}$$

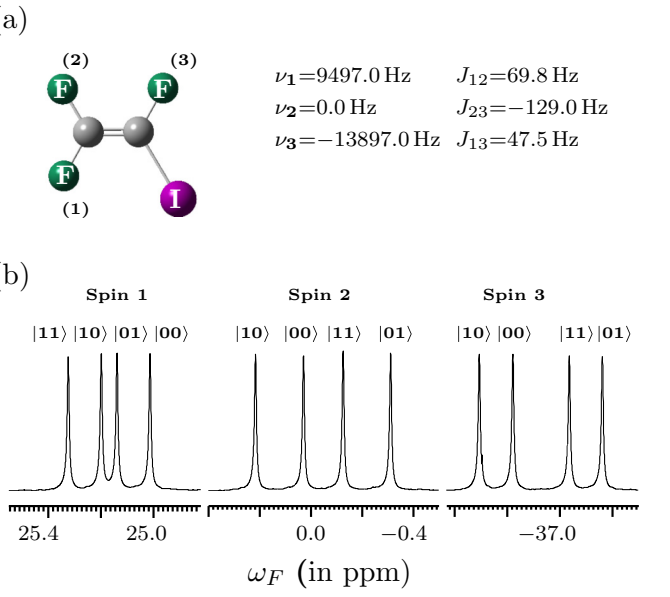

FIG. 2. (Color online) (a) Molecular structure and NMR parameters (chemical shifts and J coupling in Hz) and ^{19}F NMR spectrum of trifluoroiodoethylene. The three fluorine spins correspond to the three-qubit system. (b) The 1D ^{19}F NMR thermal equilibrium spectrum obtained after a $\frac{\pi}{2}$ readout pulse. The NMR transitions of each qubit are labeled by the corresponding logical states of the other two qubits.

can hence be obtained by normalizing the deviation density matrix ($\rho_{\rm dev} = \rho_{000} - \rho_{\rm I}$) by the factor ϵ and adding ρ_I to it [35]. The experimentally obtained density matrices were tomographed by standard state tomography procedures [36–38]. The three-qubit experimental density matrix was tomographed using a set of eleven detection operators defined by {III, IIX, IXI, XII, IIY, IYI, YII, YYI, IXX, XXX, YYY}, and the two, two-qubit reduced density matrices were determined using a set of four detection operators defined by {III, IXI, IYI, XXI} and {III, IIX, IIY, IXX}, respectively, with I denoting the identity (or no-operation) operator and X(Y) denoting a spin-selective $\frac{\pi}{2}$ pulse of X(Y) phase on a specified qubit. The fidelity of the reconstructed state was computed using the Uhlmann-Jozsa fidelity measure [39,40]:

$$F = [\mathrm{Tr}(\sqrt{\sqrt{\rho_{\rm theory}}\rho_{\rm expt}\sqrt{\rho_{\rm theory}}})]^2, \tag{15}$$

where $\rho_{\rm theory}$ and $\rho_{\rm expt}$ denote the theoretical and experimental density matrices, respectively.

A. $W\bar{W}$ construction scheme

The circuit to construct a $W\bar{W}$ state consists of several single-qubit and two-qubit gates. A single-qubit gate, $U_i[\alpha]_y$, acting on the ith qubit, achieves a rotation by the angle α around the y axis with a corresponding unitary matrix given by

$$U_i[\alpha]_y = \begin{pmatrix} \cos\frac{\alpha}{2} & -\sin\frac{\alpha}{2} \\ \sin\frac{\alpha}{2} & \cos\frac{\alpha}{2} \end{pmatrix}. \tag{16}$$

A two-qubit controlled-rotation gate $\mathrm{CR}_{ij}[\phi]_y$, implements the single-qubit rotation $U_j[\phi]_y$ on the target qubit j about the y axis, if the control qubit i is in the state $|1\rangle$. The CNOT_{ij} gate implements a controlled-NOT operation with the ith qubit as the control and the jth qubit as the target.

The sequence of gates to construct a $W\bar{W}$ state, starting from the initial pseudopure state $|000\rangle$, is given as follows:

$$|000\rangle$$
$$\downarrow \boxed{U_1[-\tfrac{\pi}{3}]_y} \downarrow$$
$$\tfrac{1}{2}\left(\sqrt{3}|000\rangle - |100\rangle\right)$$
$$\downarrow \boxed{\mathrm{CR}_{12}\left[2\cos^{-1}(1/\sqrt{3})\right]_y} \downarrow$$
$$\tfrac{1}{2}\left(\sqrt{3}|000\rangle - \tfrac{1}{\sqrt{3}}|100\rangle - \sqrt{\tfrac{2}{3}}|110\rangle\right)$$
$$\downarrow \boxed{\mathrm{CR}_{21}[-\tfrac{\pi}{2}]_y} \downarrow$$
$$\tfrac{1}{2}\left(\sqrt{3}|000\rangle - \tfrac{1}{\sqrt{3}}(|100\rangle + |110\rangle + |010\rangle)\right)$$
$$\downarrow \boxed{\mathrm{CNOT}_{13}} \downarrow$$
$$\tfrac{1}{2}\left(\sqrt{3}|000\rangle - \tfrac{1}{\sqrt{3}}(|101\rangle + |111\rangle + |010\rangle)\right)$$
$$\downarrow \boxed{\mathrm{CNOT}_{23}} \downarrow$$
$$\tfrac{1}{2}\left(\sqrt{3}|000\rangle - \tfrac{1}{\sqrt{3}}(|101\rangle + |110\rangle + |011\rangle)\right)$$
$$\downarrow \boxed{U_1[\tfrac{\pi}{2}]_y U_2[\tfrac{\pi}{2}]_y U_3[\tfrac{\pi}{2}]_y} \downarrow$$
$$\tfrac{1}{\sqrt{6}}(|001\rangle + |010\rangle + |011\rangle + |100\rangle + |101\rangle + |110\rangle).$$

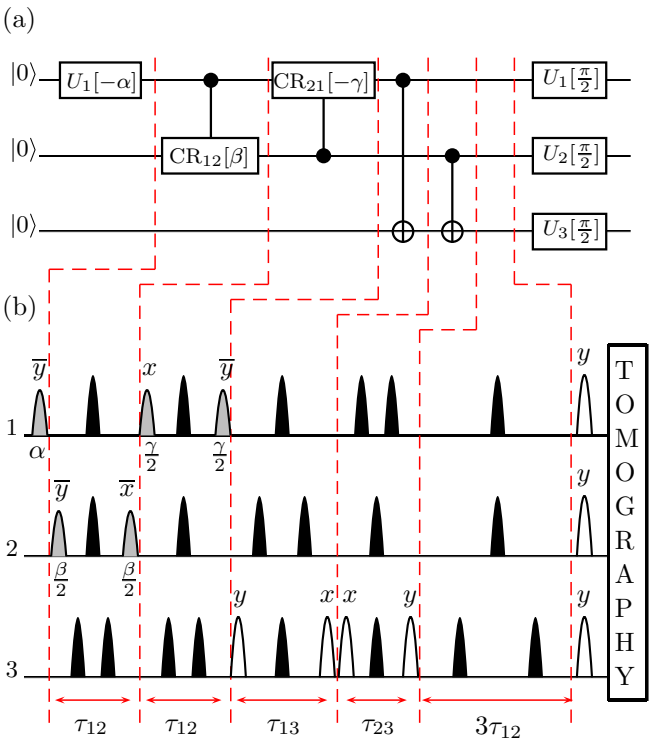

FIG. 3. (Color online) (a) Quantum circuit showing the sequence of gates required to construct the $W\bar{W}$ state, starting from the pseudopure state $|000\rangle$. The gate operations are described in the main text and all the rotations take place about the y axis. (b) NMR pulse sequence to create a $W\bar{W}$ state. All the pulses are low-power selective pulses represented by shaped blocks. Solid black shapes are π refocusing pulses, white shapes correspond to pulses of $\frac{\pi}{2}$ flip angle, and the gray shaded shapes are labeled with their specific flip angles and phases. The axes of rotation are specified at the top of each pulse. Vertical dotted red lines show the correspondence between the quantum circuit and the experimental pulse sequence. All pulses are of phase x unless otherwise labeled. The values of the rf pulse flip angles used are $\alpha = \frac{\pi}{3}$, $\beta = 2\cos^{-1}(\frac{1}{\sqrt{3}})$, and $\gamma = \frac{\pi}{2}$, and τ_{ij} represents an evolution under the J_{ij} coupling. The last $3\tau_{12}$ period is used to compensate the extra phase acquired (as described in the text).

The quantum circuit to construct the $W\bar{W}$ state on a three-qubit system is given in Fig. 3(a).

The NMR pulse sequence to create the $W\bar{W}$ state, starting from the pseudopure state $|000\rangle$ is given in Fig. 3(b). All the pulses are shaped pulses, labeled by the corresponding axes of rotation and the flip angles; τ_{ij} denotes an evolution period under the J_{ij} coupling. Refocusing (π) pulses are applied in the middle of the evolution periods to compensate for chemical shift evolution and pairs of π pulses are introduced at 1/4 and 3/4 of the evolution periods to eliminate undesired J evolutions. After the evolution interval τ_{23} and the $[\frac{\pi}{2}]_y$ on the third qubit (corresponding to a CNOT_{23} gate), the state obtained is $\frac{\sqrt{3}}{2}|000\rangle - \frac{1}{2\sqrt{3}}(\iota|101\rangle + |110\rangle + \iota|011\rangle)$. There is an undesirable extra relative phase of "ι" that has accumulated between two of the basis vectors. This undesired extra phase factor is compensated for during the evolution interval $3\tau_{12}$. The implementation of the last module (simultaneous $[\frac{\pi}{2}]_y$

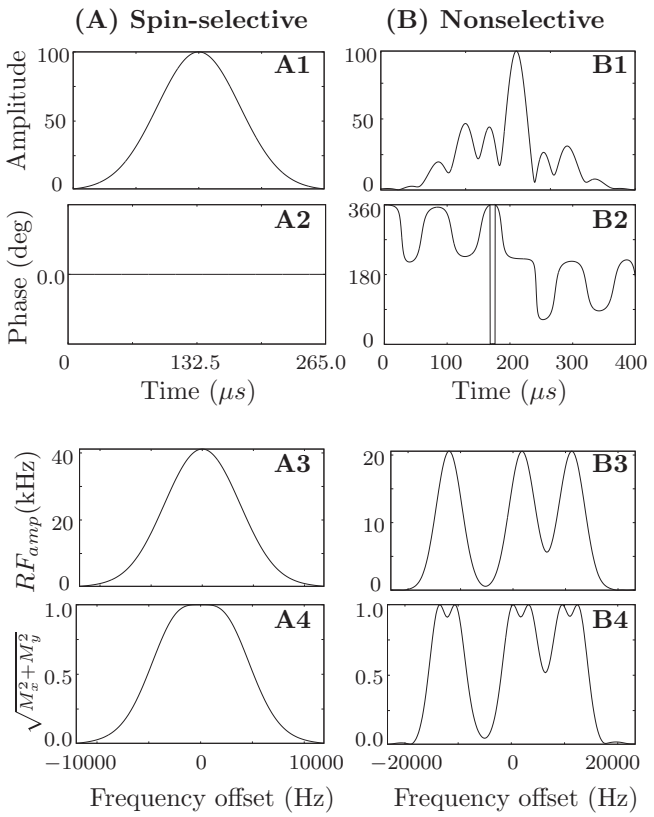

FIG. 4. (A1,B1) Normalized amplitude and (A2,B2) phase time-domain profiles of a spin-selective and a nonselective rf pulse, respectively. (A3,B3) Frequency-domain pulse profile versus frequency offset of a spin-selective and a non-selective rf pulse, respectively. (A4,B4) Simulated magnetization excitation profiles versus frequency offset in response to a 90° spin-selective and a nonselective rf pulse, respectively.

pulses on all the three qubits) results in the desired $W\bar{W}$ state with no extra relative phase. Spin-selective excitation was achieved using Gaussian-shaped pulses of duration 265 μs, digitized with 1000 points, and exciting a bandwidth of 8000 Hz. The pulse profiles are robust with good selectivity and give rise to a uniform spin response in the desired frequency range. The excitation profile of the shaped pulse is uniform up to 6000 Hz of the bandwidth, with very low intensity tails extending up to $\pm$10 000 Hz. The three fluorine spins resonate over a very large bandwidth of 68 ppm and hence uniform nonselective excitation cannot be achieved by a single nonselective pulse. The nonselective excitation rf pulse we designed comprises a set of three Gaussian shaped pulses that are applied at different spin frequency offsets and frequency modulated to achieve simultaneous excitation. This shaped pulse is of 400 μs in duration, digitized by 1500 points. The pulse excites bandwidths of 5000 Hz centered at the three spin frequency offsets (9497, 0, and $-$13 897 Hz, with the zero-frequency offset being on-resonance) and achieves an almost hat-shaped excitation profile around the respective resonance frequency offsets. Figure 4 depicts simulations of the shaped rf pulse profiles to investigate their rf amplitude and frequency offset sensitivity, with panels A and B showing details of a selective and a nonselective rf pulse, respectively.

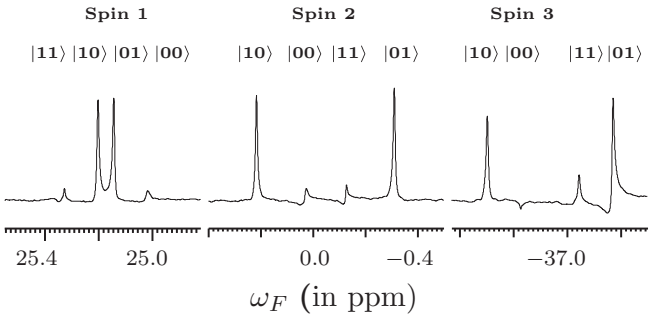

FIG. 5. The one-dimensional ^{19}F NMR spectrum corresponding to the creation of the $W\bar{W}$ state. The NMR transitions of each qubit are labeled by the corresponding logical states of the other two qubits.

Figures 4(A1) and 4(A2) show the pulse shape profile in the time domain with normalized amplitude and phase profiles for a spin-selective rf pulse, while Figs. 4(B1) and 4(B2) show the same profiles for a nonselective rf pulse. The frequency domain profiles in Figs. 4(A3) and 4(B3) are the Fourier transformations of the shaped pulses, with spectral amplitude and phase plotted versus the frequency offset for a spin-selective and a nonselective rf pulse, respectively. Figures 4(A4) and 4(B4) depict the excitation profile corresponding to a 90° excitation pulse versus frequency offset, where M_x and M_y are the x and y components of the magnetization vector. The spin response was simulated for a single-spin Bloch model using the Bruker NMRSIM package.

The NMR spectrum of the $W\bar{W}$ state obtained by a sequence of selective rotations on the initial pseudopure state is shown in Fig. 5. Each spin multiplet has two resonance peaks (as compared to four resonance peaks for the thermal equilibrium state). The expected NMR spectral pattern of an ideal $W\bar{W}$ state should contain resonance peaks of equal magnitude and phase, and deviations from ideal spectral peak intensities and phases in the experimentally obtained spectrum can be attributed to imperfections in the rf pulse calibrations and to relaxation during the selective pulse durations.

The tomograph of the experimentally constructed $W\bar{W}$ state is shown in Fig. 6. The experimentally tomographed state was compared with the theoretically expected state and the density matrices match well, within experimental error, with a computed state fidelity of 0.96 [the fidelity was computed from Eq. (15)].

B. Reconstruction of $W\bar{W}$ from two-party reduced density matrices

A protocol was developed [12] to validate the surprising aspect of multiparty correlations asserted by Linden *et al.* [9,41] that the information about three-party correlations of almost all pure three-qubit states (except for GHZ-type states) is already contained in their corresponding two-party reduced states. We delineate below the argument for how a general three-qubit pure state, ρ_{ABC}, can be completely determined by using any of the equivalent sets (ρ_{AB},ρ_{AC}), (ρ_{AB},ρ_{BC}), or (ρ_{AC},ρ_{BC}) of reduced two-party states. The reduced single-qubit reduced state ρ_A and the two-qubit reduced state ρ_{BC} share the same

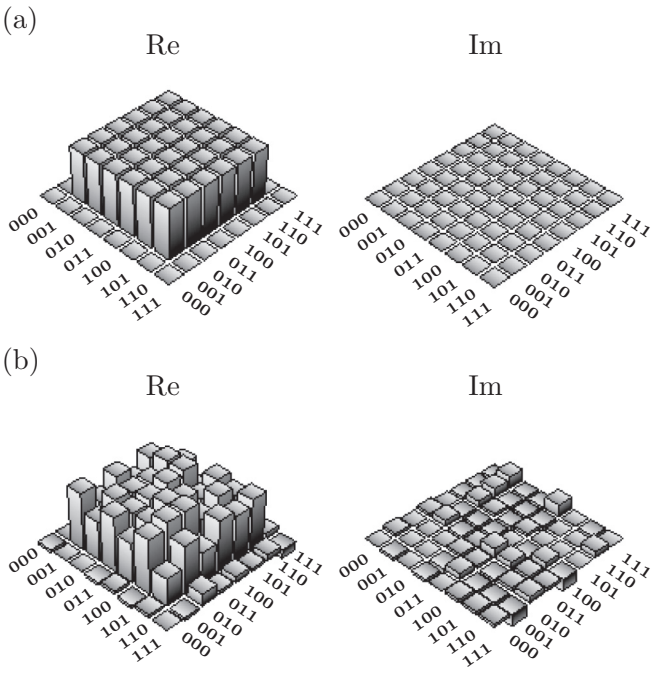

FIG. 6. The real (Re) and imaginary (Im) parts of the (a) theoretically expected and (b) experimental density matrices for the $W\bar{W}$ state reconstructed using full state tomography. The rows and columns of the bar graphs depict the computational basis of the three qubits in binary order from $|000\rangle$ to $|111\rangle$. The experimentally tomographed state has a fidelity of 0.96.

set of eigenvalues and can hence be written as [12]

$$\rho_A = \sum_i p_A^i |i\rangle\langle i|,$$
$$\rho_{BC} = \sum_i p_A^i |i;BC\rangle\langle i;BC|, \tag{17}$$

where $\{|i\rangle\}$ are the eigenvectors of ρ_A with eigenvalues $\{p_A^i\}$, and $\{|i;BC\rangle\}$ are the eigenvectors of ρ_{BC} with eigenvalues $\{p_A^i\}$. Furthermore, the three-qubit pure states that are compatible with ρ_A and ρ_{BC} are given by

$$|\psi_{ABC};\alpha\rangle = \sum_i e^{\iota\alpha_i}\sqrt{p_A^i}|i\rangle \otimes |i;BC\rangle. \tag{18}$$

Similarly, the three-qubit pure states that are compatible with ρ_C and ρ_{AB} are given by

$$|\psi_{ABC};\gamma\rangle = \sum_k e^{\iota\gamma_k}\sqrt{p_c^k}|k;AB\rangle \otimes |k\rangle, \tag{19}$$

where $\{|k\rangle\}$ are the eigenvectors of ρ_C with eigenvalues $\{p_c^k\}$, and $\{|k;AB\rangle\}$ are the corresponding eigenvectors of ρ_{AB}. Since the pure state $|\psi_{ABC}\rangle$ is compatible with both ρ_{AB} and ρ_{BC}, we can now consistently find the values of α_i and γ_k while ensuring that $|\psi_{ABC};\alpha\rangle = |\psi_{ABC};\gamma\rangle$.

We used the set of two, two-party reduced states (ρ_{AB},ρ_{BC}), to reconstruct the full three-qubit $W\bar{W}$ state. The reconstructed density matrix for the $W\bar{W}$ state, using two sets of the corresponding two-qubit reduced density matrices (ρ_{AB},ρ_{BC}),

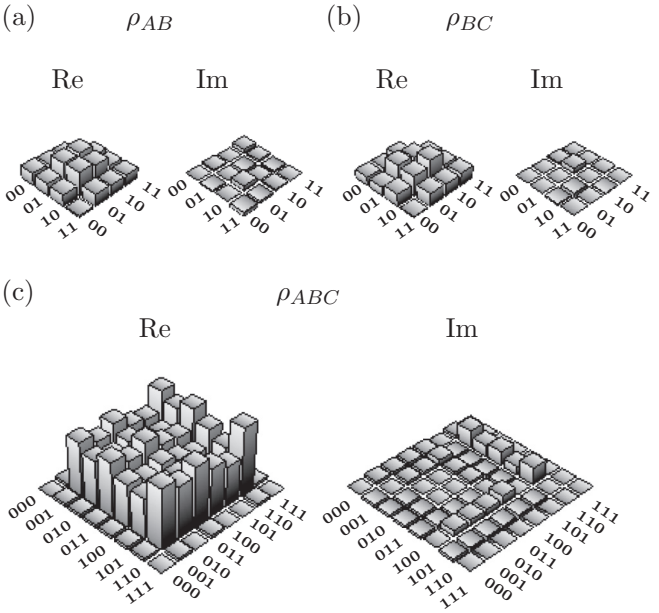

FIG. 7. The real (Re) and imaginary (Im) parts of the tomographed density matrix for the $W\bar{W}$ state. (a) The two-qubit reduced density matrix ρ_{AB}. (b) The two-qubit reduced density matrix ρ_{BC}. (c) The entire three-qubit density matrix ρ_{ABC}, reconstructed from the corresponding two-qubit reduced density matrices. The rows and columns in the bar graphs encode the computational basis of the qubits, from $|00\rangle$ to $|11\rangle$ for two qubits and from $|000\rangle$ to $|111\rangle$ for three qubits. The fidelity between the three-qubit state (ρ_{ABC}) reconstructed from the two-qubit density matrices and the three-qubit state obtained by complete three-qubit state tomography is found to be 0.91.

is given in Fig. 7. The two-party reduced states were able to reconstruct the three-party $W\bar{W}$ state with a fidelity of 0.91, which matches well with the full reconstruction of the entire three-qubit state given in Fig. 6(b).

IV. CONCLUSIONS

We described a measurement-based filtration scheme to demonstrate the ILO equivalence of the $W\bar{W}$ state with the GHZ state. We experimentally implemented an NMR-based scheme to construct a $W\bar{W}$ state. We were able to show that the three-qubit density operator ρ_{ABC} obtained by full state tomography matches well with the same three-qubit state reconstructed using a set of two-party reduced density operators (ρ_{AB},ρ_{BC}). Thus, although the $W\bar{W}$ state belongs to the same entanglement class as the GHZ state, the two states store information about multiparty correlations in completely different ways. We thus experimentally demonstrated an interesting feature of multiqubit entanglement, namely, that two different entangled states belonging to the same SLOCC class can still have their correlations exhibiting contrasting irreducible properties.

Since distinguishing entangled states is still a hard task, our work can be used as a benchmark to further classify how different entangled states store information about their

correlations. Our work also has important implications for comparing the utility of different kinds of entangled states to perform the same computational task. We were unable to find a suitable molecular architecture to experimentally implement the ILO, since this requires each of the three qubits to be coupled to a separate one-qubit ancilla. However, it is a worthwhile exercise to look for an experimental implementation of the filtering protocol to perform the ILO. A further issue with such an implementation is the involvement of projective measurements, which are not straightforward to achieve using NMR.

ACKNOWLEDGMENTS

All experiments were performed on a Bruker Avance-III 400 MHz FT-NMR spectrometer at the NMR Research Facility at IISER Mohali. S.D. acknowledges financial support from the University Grants Commission (UGC) India.

[1] R. Horodecki, P. Horodecki, M. Horodecki, and K. Horodecki, Rev. Mod. Phys. **81**, 865 (2009).
[2] O. Gühne and G. Töth, Phys. Rep. **474**, 1 (2009).
[3] C. Eltschka and J. Siewert, J. Phys. A **47**, 424005 (2014).
[4] J. I. de Vicente, T. Carle, C. Streitberger, and B. Kraus, Phys. Rev. Lett. **108**, 060501 (2012).
[5] M.-J. Zhao, T.-G. Zhang, X. Li-Jost, and S.-M. Fei, Phys. Rev. A **87**, 012316 (2013).
[6] A. Acin, A. Andrianov, L. Costa, E. Jane, J. I. Latorre, and R. Tarrach, Phys. Rev. Lett. **85**, 1560 (2000).
[7] H. Kampermann, O. Gühne, C. Wilmott, and D. Bruß, Phys. Rev. A **86**, 032307 (2012).
[8] L. Chen and Y. X. Chen, Phys. Rev. A **74**, 062310 (2006).
[9] N. Linden, S. Popescu, and W. K. Wootters, Phys. Rev. Lett. **89**, 207901 (2002).
[10] S. N. Walck and D. W. Lyons, Phys. Rev. Lett. **100**, 050501 (2008).
[11] S. N. Walck and D. W. Lyons, Phys. Rev. A **79**, 032326 (2009).
[12] L. Diosi, Phys. Rev. A **70**, 010302 (2004).
[13] D. Cavalcanti, L. M. Cioletti, and M. O. Terra Cunha, Phys. Rev. A **71**, 014301 (2005).
[14] P. Parashar and S. Rana, Phys. Rev. A **80**, 012319 (2009).
[15] C. F. Roos, M. Riebe, H. Haffner, W. Hansel, J. Benhelm, G. P. T. Lancaster, C. Becher, F. Schmidt-Kaler, and R. Blatt, Science **304**, 1478 (2004).
[16] H. Mikami, Y. Li, K. Fukuoka, and T. Kobayashi, Phys. Rev. Lett. **95**, 150404 (2005).
[17] K. J. Resch, P. Walther, and A. Zeilinger, Phys. Rev. Lett. **94**, 070402 (2005).
[18] S. Bugu, C. Yesilyurt, and F. Ozaydin, Phys. Rev. A **87**, 032331 (2013).
[19] C. Yesilyurt, S. Bugu, and F. Ozaydin, Quantum Inf. Process. **12**, 2965 (2013).
[20] F. Ozaydin, S. Bugu, C. Yesilyurt, A. A. Altintas, M. Tame, and S. K. Ozdemir, Phys. Rev. A **89**, 042311 (2014).
[21] R. Laflamme, E. Knill, W. H. Zurek, P. Catasti, and S. V. S. Mariappan, Phil. Trans. Roy. Soc. Lond. A **356**, 1941 (1998).
[22] R. J. Nelson, D. G. Cory, and S. Lloyd, Phys. Rev. A **61**, 022106 (2000).
[23] G. Teklemariam, E. M. Fortunato, M. A. Pravia, Y. Sharf, T. F. Havel, D. G. Cory, A. Bhattaharyya, and J. Hou, Phys. Rev. A **66**, 012309 (2002).
[24] M. Kawamura, T. Morimoto, Y. Mori, R. Sawae, K. Takarabe, and Y. Manmoto, Int. J. Quantum Chem. **106**, 3108 (2006).
[25] X. Peng, J. Zhang, J. Du, and D. Suter, Phys. Rev. A **81**, 042327 (2010).
[26] Y. Gao, H. Zhou, D. Zou, X. Peng, and J. Du, Phys. Rev. A **87**, 032335 (2013).
[27] S. Dogra, K. Dorai, and Arvind, Phys. Rev. A **91**, 022312 (2015).
[28] Z. Gedik, Opt. Commun. **284**, 681 (2011).
[29] A. R. Usha Devi, Sudha, and A. K. Rajagopal, Quant. Inf. Proc. **11**, 685 (2012).
[30] Sudha, A. R. Usha Devi, and A. K. Rajagopal, Phys. Rev. A **85**, 012103 (2012).
[31] N. Gisin, Phys. Lett. A **210**, 151 (1996).
[32] F. Verstraete and M. M. Wolf, Phys. Rev. Lett. **89**, 170401 (2002).
[33] D. Das, R. Sengupta, and Arvind, arXiv:1504.02991.
[34] D. Cory, M. Price, and T. Havel, Physica D (Amsterdam, Neth.) **120**, 82 (1998).
[35] A. Gavini-Viana, A. M. Souza, D. O. Soares-Pinto, J. Teles, R. S. Sarthour, E. R. deAzevedo, T. J. Bonagamba, and I. S. Oliveira, Quantum Inf. Process. **9**, 575 (2009).
[36] I. L. Chuang, N. Gershenfeld, M. Kubinec, and D. W. Leung, Proc. Roy. Soc., Ser. A **454**, 447 (1998).
[37] G. Long, H. Yan, and Y. Sun, J. Opt. B **3**, 376 (2001).
[38] G. M. Leskowitz and L. J. Mueller, Phys. Rev. A **69**, 052302 (2004).
[39] A. Uhlmann, Rep. Math. Phys. **9**, 273 (1976).
[40] R. Jozsa, J. Mod. Opt. **41**, 2315 (1994).
[41] N. Linden and W. K. Wootters, Phys. Rev. Lett. **89**, 277906 (2002).